

RESEARCH

Open Access



Integrated network pharmacology reveals the mechanism of action of Xianlinggubao prescription for inflammation in osteoarthritis

Jingyi Hou¹, Yubo Li², Yu Zhang², Ning Yang², Bin Chen², Guiyun Ma^{2*} and Naiqiang Zhu^{2,3*}

Abstract

Background Osteoarthritis (OA), a leading cause of disability worldwide, is characterized by complex interactions between cartilage degradation and synovial inflammation. While NSAIDs are the primary treatment, their prolonged use exacerbates gastrointestinal risks and does not alter disease progression. Xianlinggubao (XLGB), an approved Chinese herbal remedy for osteoporosis, has demonstrated promising anti-osteoarthritic effects in preliminary studies. However, its multi-component mechanisms targeting OA-related inflammation require further clarification. This study integrates network pharmacology with experimental validation to investigate XLGB's anti-inflammatory mechanisms in OA.

Methods Bioactive compounds of XLGB and their respective targets were sourced from the TCMS, ETCM, SymMap, and ChEMBL databases. Targets linked to OA-related inflammation were identified through differential expression analysis and by querying OMIM, GeneCards, and PubMed Gene databases. Network pharmacology and bioinformatics approaches were employed to construct compound-target and protein-protein interaction (PPI) networks, enabling the identification of pivotal therapeutic targets. Functional enrichment of these targets was performed using the ClusterProfiler package in R. The binding affinity of compounds to anti-inflammatory OA targets was assessed through molecular docking, dynamics simulations, RT-PCR, and immunofluorescence assays.

Results Fifty-five bioactive compounds corresponding to 475 XLGB targets and 125 genes involved in OA-related inflammation were identified. PPI network analysis revealed that XLGB may alleviate OA inflammation by modulating key genes, including COX-2, IL-1 β , TNF, IL-6, and MMP-9. Molecular simulations indicated strong binding affinities between bioactive compounds in XLGB and these critical targets. Functional enrichment analysis suggested that XLGB's anti-inflammatory action in OA may involve regulation of pathways such as IL-17, TNF, and NF- κ B. In vitro experiments further confirmed that XLGB mitigates OA inflammation by modulating these genes, proteins, and signaling pathways.

Conclusions Through network pharmacology, this study elucidated the mechanisms of XLGB in OA inflammation, highlighting its modulation of IL-6, IL-1 β , TNF- α , PTGS2, MMP-9, and the NF- κ B pathway. These findings provide strong support for the clinical application of XLGB in managing OA-related inflammation.

*Correspondence:

Guiyun Ma
maguiyun3778@163.com
Naiqiang Zhu
zhunq2010@163.com

Full list of author information is available at the end of the article



© The Author(s) 2025. **Open Access** This article is licensed under a Creative Commons Attribution-NonCommercial-NoDerivatives 4.0 International License, which permits any non-commercial use, sharing, distribution and reproduction in any medium or format, as long as you give appropriate credit to the original author(s) and the source, provide a link to the Creative Commons licence, and indicate if you modified the licensed material. You do not have permission under this licence to share adapted material derived from this article or parts of it. The images or other third party material in this article are included in the article's Creative Commons licence, unless indicated otherwise in a credit line to the material. If material is not included in the article's Creative Commons licence and your intended use is not permitted by statutory regulation or exceeds the permitted use, you will need to obtain permission directly from the copyright holder. To view a copy of this licence, visit <http://creativecommons.org/licenses/by-nc-nd/4.0/>.

Keywords Bioinformatics analysis, Hub gene, Network pharmacology, NF- κ B, Osteoarthritis, Xianlinggubao prescription

Introduction

Osteoarthritis (OA) is a prevalent age-related degenerative joint disorder, characterized by progressive articular cartilage degradation, accompanied by subchondral bone sclerosis and pathological remodeling [1, 2]. However, the precise etiological mechanisms driving OA pathogenesis remain incompletely understood. Current clinical management predominantly involves pharmacological interventions, such as nonsteroidal anti-inflammatory drugs (NSAIDs) and opioid analgesics [3, 4], alongside surgical procedures like osteotomy, arthroplasty, and arthrodesis [5, 6]. These treatments, however, are frequently associated with adverse effects, including surgical complications and cardiovascular risks [4, 7, 8]. Given that OA is linked to a persistent inflammatory response within joint tissues, driven by various immune cells, further understanding of the interactions between pro-inflammatory cytokines and immune cells is critical to elucidating its pathogenesis. Inflammatory cytokines and chemokines, synovial responses, immune cell infiltration, and the activation of inflammatory pathways all contribute to OA progression.

Traditional Chinese medicine (TCM) has been widely employed in clinical practice for managing OA due to its minimal side effects, substantial efficacy, and cost-effectiveness [9]. Xianlinggubao Prescription (XLGB), composed of six herbs—Yinyanghuo (*Epimedium brevicornu* Maxim., 70%), Zhimu (*Anemarrhena asphodeloides* Bunge, 5%), Danshen (*Salvia miltiorrhiza* Bunge, 5%), Buguzhi (*Cullen corylifolium* (L.) Medik., 5%), Xuduan (*Dipsacus asperoides* C.Y.Cheng & T.M.Ai, 10%), and Dihuang (*Rehmannia glutinosa* (Gaertn.) DC., 5%)—has shown effectiveness in treating conditions such as osteoporosis, aseptic osteonecrosis, OA, and bone fractures. Clinical studies suggest that XLGB enhances superoxide dismutase activity, reduces malondialdehyde and nitric oxide (NO) levels, and suppresses the expression of sensitive biomarkers such as C-reactive protein, TNF- α , and IL-6 in patients with OA [10]. However, the active components and specific anti-inflammatory targets of XLGB in OA remain unclear.

Systems pharmacology approaches, incorporating systems biology, cheminformatics, bioinformatics, multidirectional network biology, and traditional pharmacology [11], have been employed to identify bioactive compounds in TCM formulations and predict their mechanisms of action. In this study, network pharmacology, combined with bioinformatics analysis, was utilized

to predict XLGB's anti-inflammatory targets in OA, with subsequent validation of these targets to provide insights for future clinical applications (Fig. 1).

Materials & methods

Chemicals and materials

XLGB Prescription was purchased from Tongjitang Pharmacy (Guizhou, China, No. X742603), while Lipopolysaccharide (LPS, L2880) was sourced from Sigma-Aldrich (St. Louis, MO, USA). High-quality fetal bovine serum (HI-FBS, 10,099,141) and Dulbecco's Modified Eagle Medium (DMEM, 11,965,092) were obtained from GIBCO (Grand Island, NY, USA). The Griess reagent system (S0021), Cy3-labeled Goat antibody (A0516), DAPI (C1002), and CellTiter-Lumi™ Plus Detection Kit (C0065) were acquired from Beyotime (Beijing, China). TRIzol reagent (15,596,026) and real-time PCR kits (RR820 A) were purchased from Invitrogen Inc. (Carlsbad, CA, USA) and Takara Biotechnology Co., Ltd (Kusatsu, Japan), respectively. NF- κ B p65 antibodies (AF0246) were obtained from Affinity (China). RAW264.7 cells were purchased from the Cell Culture Center of the Chinese Academy of Medical Sciences (Beijing, China). Methanol (1.06035.2500), acetonitrile (1.00029.2500), and formic acid (1.00264.1000), all of LC-MS grade, were sourced from Merck KGaA (Germany). All solvents used for reagent preparation were of chromatographic grade.

Collection of chemical ingredients for XLGB

All chemical components for XLGB were retrieved from the Traditional Chinese Medicine Systems Pharmacology Database (TCMSP) [12], the Encyclopedia of Traditional Chinese Medicine (ETCM) [13], and SymMap [14]. To identify bioactive ingredients, drug-likeness (DL) and oral bioavailability (OB) were employed as screening criteria [15]. Active components were selected based on an OB threshold of $\geq 30\%$ and a DL threshold of ≥ 0.18 .

Prediction of targets of bioactive compounds

Targets associated with the candidate bioactive compounds were identified using the STITCH, Similarity Ensemble Approach (SEA) [16], SymMap, and ChEMBL databases [17], with the "Homo sapiens" setting. Genetic data, including gene names, IDs, and organism details, were retrieved from UniProt (<https://www.uniprot.org/>) [18]. The identified targets are listed in Table S1.

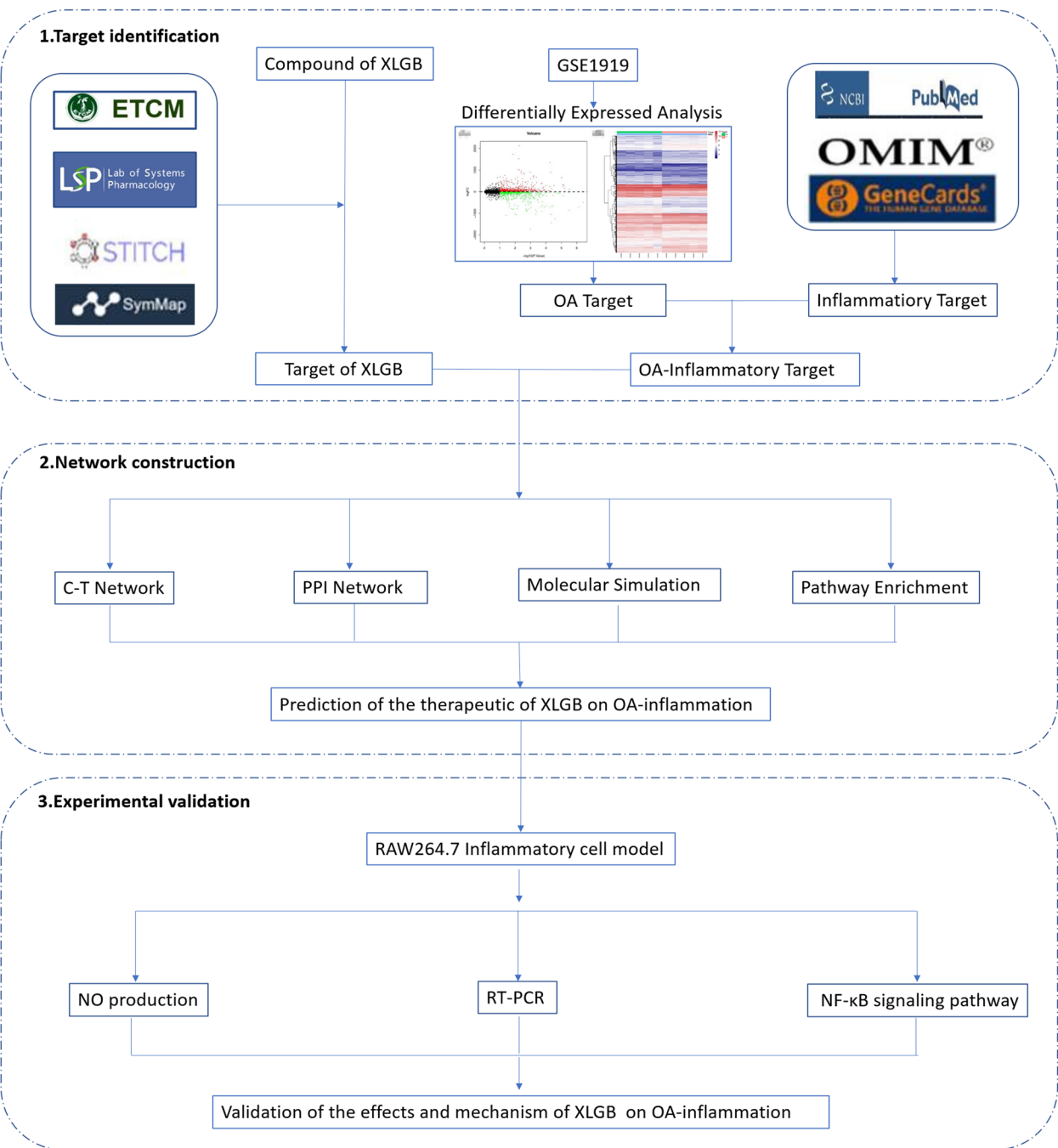


Fig. 1 Schematic representation of a pharmacology-based approach to investigate the therapeutic mechanisms of Xianlinggubao (XLGB) on OA inflammation, integrating target identification, network analysis, and experimental validation

Identification of OA and inflammation-related targets

OA-related targets were identified by screening differentially expressed genes (DEGs) from the GSE1919 dataset, as described by Ungethuem et al. (PMID: 20,858,714) [19]. The GSE1919 dataset, which includes 15 synovial tissue samples—five from patients with OA,

five from patients with rheumatoid arthritis (RA), and five from healthy controls—was downloaded from the GEO database. Data were generated using the Affymetrix Human Genome U95 A Array and subsequently annotated to match gene probes to gene names. Differential gene expression analysis was performed using

the "limma" package in R [20], with a cutoff of $p < 0.05$ and $|\log_2 \text{fold change (FC)}| \geq 2$. The "anti-inflammatory," "inflammatory," and "inflammation" datasets were then imported into the OMIM, GeneCards, and PubMed Gene databases to obtain inflammation-related targets. The FunRich [21] online tool was employed to identify overlapping DEGs and inflammation-related genes, yielding OA-inflammatory targets.

Network construction

To elucidate the molecular mechanism of XLGB in OA treatment, a multi-layered network was constructed: First, TCM compounds were linked to their respective targets, creating a compound-target network. Next, the STRING database was utilized to establish a protein-protein interaction (PPI) network encompassing OA inflammation-related and XLGB candidate targets. This interconnected network was visualized using Cytoscape 3.7.2 software, and topological properties were analyzed through the "Network Analysis" plug-in [22].

Hub gene analysis

The "CytoHubba" plug-in was employed to assess the topological characteristics of network nodes, identifying hub genes most likely to counteract XLGB's inflammatory effects in OA. The DisGenet database [23], a platform detailing biological mechanisms, was used to extract gene and target (protein) data related to human diseases.

Functional enrichment analysis

Gene Ontology, Functional Annotation, and KEGG Pathway Analysis of gene clusters were conducted using the ClusterProfiler package in R for functional evaluation [24].

Molecular docking and dynamics simulation

Molecular docking was performed as previously outlined [25]. Briefly, the bioactive components and protein structures of the hub genes were retrieved from the PubChem and PDB databases, including PTGS2 (PDB ID: 5F19), IL-1 β (PDB ID: 6Y8M), TNF- α (PDB ID: 2AZ5), IL-6 (PDB ID: 4O9H), and MMP-9 (PDB ID: 1ITV). Docking scores assessed the binding affinity between ingredients and predicted hub genes. Additionally, molecular dynamics (MD) simulations were conducted to confirm binding energy and ligand stability. Initial conformations for MD simulations were derived from docking results. Small molecules were optimized using ORCA [26] with DFT (B3LYP/def2-TZVP) [27–29], followed by RESP2 electrostatic potential fitting via Multiwfn [30]. Drug parameter files were generated using the GAFF force field [31] with sobtop, while protein structures

were processed with PDBFixer to repair missing atoms and optimize protonation states. MD simulations were conducted in GROMACS (version 2025.0) [32] for 100 ns per protein-drug complex. Systems were parameterized using AMBER ff14SB (protein) and GAFF (drug) [31, 33], solvated in TIP3P water with 0.15 M NaCl [34, 35], and neutralized with counterions. Following steepest descent energy minimization (10,000 steps with harmonic restraints), systems underwent NVT (0–300 K over 1.0 ps) and NPT (2 ns at 300 K, 1 atm) equilibration [36]. Production runs in the NPT ensemble employed V-rescale for temperature [37], C-rescale for pressure [38], PME for electrostatic interactions [39], and LINCS for bond constraints. Binding free energies were calculated via MM/GBSA (GB-Neck2 model) [40] using 1,000 conformations (50–100 ns trajectory, 5-frame intervals), with per-residue decomposition to quantify amino acid contributions.

Preparation of XLGB extract

XLGB powder (10 g) was extracted twice with five times the amount of pure water under reflux for 30 min. The resulting extract was concentrated using rotary evaporation and then diluted to appropriate concentrations with PBS.

UPLC/TOF-MS analysis

UPLC chromatography

Separation of the extract was performed using a Thermo Vanquish UHPLC system equipped with a Zorbax Eclipse C18 column (2.1 \times 100 mm, 1.8 μ m). The mobile phase consisted of 0.1% formic acid aqueous solution (solvent A) and acetonitrile (solvent B). The gradient elution procedure was as follows: 0–2 min 0–5%; 2–6 min 5–30%; 6–7 min 30%; 7–12 min 78%; 12–14 min 78%; and 14–17 min 78–95%. A 10 μ L sample volume was injected for analysis at a column temperature of 30 $^{\circ}$ C and a flow rate of 0.3 mL/min.

Mass chromatography

Chemical structures were analyzed using a Q-Exactive HF mass spectrometer (Thermo Fisher Scientific) with an electrospray ionization interface. The ion source settings were as follows: swelling temperature of 325 $^{\circ}$ C, peeling temperature of 350 $^{\circ}$ C, and capillary voltage set to 3.5 kV.

Cell culture and assessment of cell viability

RAW 264.7 cells were cultured in DMEM supplemented with 10% HI-FBS and maintained at 37 $^{\circ}$ C in a 5% CO₂ atmosphere. Cells (5×10^3 /well) were seeded into 96-well plates (Corning, NY, USA, 3599). After 24 h of adhesion, cells were treated with XLGB extract at concentrations of 2.5, 5, 10, and 20 μ g/mL, based on preliminary

dose–response experiments (0–50 µg/mL). Cell viability was assessed using the CellTiter-Lumi™ Plus Assay Kit according to the manufacturer’s instructions.

Measurement of NO production

NO production was measured using the Griess reagent system, as previously described [41]. Briefly, RAW 264.7 cells (1×10^4 /well) were seeded into 96-well plates and treated with LPS (0.2 µg/mL). After a 24-h incubation with pre-prepared XLGB extracts, cells were centrifuged, and supernatants were collected for NO detection according to the manufacturer’s guidelines.

Quantitative real-time PCR analysis

Total RNA extraction was performed using TRIzol reagent following the manufacturer’s guidelines. Purity was assessed via NanoDrop 2000 (Thermo Fisher, USA), yielding $A_{260}/A_{280} = 1.92 \pm 0.08$ and $A_{260}/A_{230} = 2.15 \pm 0.12$ ($n = 6$). RNA concentration was quantified using the Qubit 4.0 RNA HS Assay Kit (Thermo Fisher), resulting in 382 ± 45 ng/µL. RNA integrity was confirmed with a 28S/18S rRNA band ratio > 2.0 on a 1.5% agarose gel ($RIN > 8.0$). Prior to PCR amplification, RNA samples underwent cDNA synthesis. Reverse transcription was performed with the PrimeScript RT Kit (RR820 A, Takara, Japan) in 20 µL reactions, each containing 1 µg RNA, 4 µL 5× buffer, 1 µL Oligo(dT)18 primer (50 µM), and 1 µL enzyme mix. The reaction was conducted under the following conditions: initial incubation at 25 °C for 10 min for primer annealing, followed by 42 °C for 60 min for cDNA synthesis, and enzyme inactivation at 85 °C for 5 min. Gene expression was quantified using the SYBR PCR Master Mix, with primers for the target genes listed in Table 1. The thermocycling protocol was as follows: 95 °C for 3 min; 40 cycles of 95 °C for 15 s, gene-specific

annealing temperature for 30 s, and 72 °C for 30 s; final extension at 72 °C for 5 min. Specificity was confirmed by melting curve analysis (60–95 °C, 0.3 °C/s). β-actin was used as an endogenous control, with triplicate technical replicates.

Immunofluorescence

Immunofluorescence assays were performed as previously described [41]. Briefly, cells were stimulated with LPS and treated with 20 µg/mL XLGB extract. Cells were fixed with 4.0% formaldehyde, permeabilized with 0.1% Triton X-100, and incubated overnight with an anti-p65 NF-κB antibody (1:100, 3% BSA). Following incubation with Cy3-labeled goat anti-rabbit IgG for 1 h, cells were stained with DAPI for 10 min.

Statistical analyses

Data analysis and graphing were conducted using Graph-Pad Prism 9 (version 9.4.0). All experiments were performed in triplicate, with data presented as the mean ± standard deviation. Group comparisons were made using one-way ANOVA and Dunnett’s post-hoc test. Statistical significance was defined as $P < 0.05$.

Results

Screening for bioactive compounds and candidate targets in XLGB

Analyses of the TCMSP, ETCM, and SymMap databases revealed 55 distinct bioactive compounds, with 12, 8, 31, 2, 5, and 3 compounds derived from the Yinyanghuo, Zhimu, Danshen, Buguzhi, Xuduan, and Dihuang species, respectively (Table 2). Target prediction conducted using the STITCH, SEA, SymMap, and ChEMBL databases identified 475 targets associated with the bioactive compounds in XLGB. These included 273, 230, 358, 34,

Table 1 Primers used for quantitative real-time PCR

Gene	Primer	Sequence (5′–3′)	GenBank	Product length
β-actin	Forward	TGTTACCAACTGGGACGACA	AJ312193.1	165
	Reverse	GGGGTGTGAAGGTCTCAAA		
PTGS2	Forward	TGAGTACCGCAAACGCTTCTC	KR709390.1	145
	Reverse	TGGACGAGGTTTTCCACCAG		
TNF-α	Forward	TAGCCAGGAGGGAGAACAGA	MH180383.1	127
	Reverse	TTTTCTGGAGGGAGATGTGG		
IL-6	Forward	CTGGAGCCCACCAAGAACGA	AB028635.1	200
	Reverse	GCCTCCGACTTGTGAAGTGGT		
MMP-9	Forward	CAAAGACCTGAAACCTCCAA	KP974687.1	59
	Reverse	GGTACAAGTATGCCTCTGCCA		
IL-1β	Forward	ATGCCACCTTTTGACAGTGATG	KY038171.1	141
	Reverse	GTTGATGTGCTGCTGCGAGATT		

Table 2 Summary of the bioactive compounds in the Xianlinggubao prescription (XLGB), including Yinyanghuo (YYH), Xuduan (XD), Danshen (DS), Dihuang (DH), Zhimu (ZM), and Buguzhi (BGZ)

Molecule Name	OB (%)	DL	Degree	Herb	Structure
Quercetin	46.43	0.28	217	YYH DS	
Icaritin	45.41	0.44	19	YYH	
8-Isopentenyl-kaempferol	37.58	0.71	13	YYH	
Icariin	41.58	0.61	19	YYH	
Luteolin	36.16	0.25	133	YYH DS	
Chryseriol	35.85	0.27	11	YYH	
C-Homoerythrinan,1,6-didehydro-3,15,16-trimethoxy	39.14	0.49	19	YYH	
Kaempferol	41.88	0.24	125	YYH ZM DS	
DFV	32.76	0.18	8	YYH	
Linoleyl acetate	42.1	0.2	7	YYH	
Poriferast-5-en-3beta-one	36.91	0.75	5	YYH	
Magnograndiolide	63.71	0.19	5	YYH	
Gentisin	64.06	0.21	39	XD	
Beta-sitosterol/Sitosterol	36.91	0.75	105	XD DH	
(E,E)-3,5-Di-O-caffeoylquinic acid	48.14	0.68	18	XD	

Table 2 (continued)

Molecule Name	OB (%)	DL	Degree	Herb	Structure
Japonine	44.11	0.25	24	XD	
Sylvestroside III	48.02	0.53	4	XD	
Asperglaucide	58.02	0.52	3	ZM	
Anhydroicaritin	45.41	0.44	24	ZM	
Timosaponin B III_qt	35.26	0.87	2	ZM	
Stigmasterol	43.83	0.76	84	ZM DH DS	
(Z)-3-(4-hydroxy-3-methoxy-phenyl)-N-[2-(4-hydroxyphenyl)ethyl]acrylamide	118.35	0.26	4	ZM	
Diosgenin	80.88	0.81	24	ZM	
Coumaroyltyramine	112.9	0.2	5	ZM	
Marmesin	50.28	0.18	9	ZM	
(2S)-7-hydroxy-2-(4-hydroxyphenyl)-8-(3-methylbut-2-enyl)chroman-4-one	36.57	0.32	8	BGZ	

Table 2 (continued)

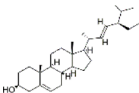
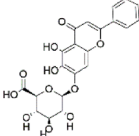
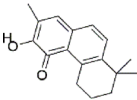
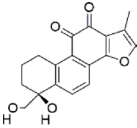
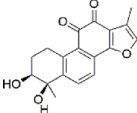
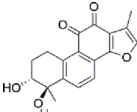
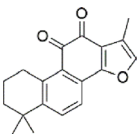
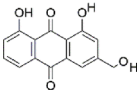
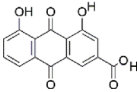
Molecule Name	OB (%)	DL	Degree	Herb	Structure
Daucosterol	20.63	0.63	26	BGZ	
Aucuboside	35.56	0.33	6	DH	
1,2,5,6-tetrahydrotanshinone	38.75	0.36	14	DS	
Poriferasterol	43.83	0.76	2	DS	
Poriferast-5-en-3beta-ol	36.91	0.75	5	DS	
Dehydrotanshinone II A	43.76	0.4	11	DS	
Baicalin	40.12	0.75	80	DS	
Digallate	61.85	0.26	2	DS	
2-isopropyl-8-methylphenanthrene-3,4-dione	36.16	0.25	37	DS	
Methylenetanshinquinone	40.86	0.23	14	DS	
Danshenol B	43.67	0.21	11	DS	

Table 2 (continued)

Molecule Name	OB (%)	DL	Degree	Herb	Structure
Danshenol A	57.95	0.56	6	DS	
Salvilenone	30.38	0.38	6	DS	
Cryptotanshinone	52.34	0.4	21	DS	
Dihydrotanshinone I	45.04	0.36	10	DS	
C09092	36.07	0.25	7	DS	
Isocryptotanshi	54.98	0.39	18	DS	
Isotanshinone II	49.92	0.4	16	DS	
Miltirone	38.76	0.25	17	DS	
1-methyl-8,9-dihydro-7H-naphtho[5,6-g]benzofuran-6,10,11-trione	34.72	0.37	11	DS	
2R)-3-(3,4-dihydroxyphenyl)-2-[(Z)-3-(3,4-dihydroxyphenyl)acryloyl]oxy-pRopionic acid	109.38	0.35	5	DS	
Salvilenone I	32.43	0.23	6	DS	

Table 2 (continued)

Molecule Name	OB (%)	DL	Degree	Herb	Structure
Salviolone	31.72	0.24	6	DS	
(6S)-6-hydroxy-1-methyl-6-methylol-8,9-dihydro-7H-naphtho[8,7-g]benzofuran-10,11-quinone	75.39	0.46	5	DS	
Tanshindiol B	42.67	0.45	4	DS	
Przewaquinone E	42.85	0.45	4	DS	
Tanshinone iia	49.89	0.4	27	DS	
Aloe-Emodin	36.91	0.75	29	DS	
Rhein	83.38	0.24	17	DS	

157, 231, and 106 targets for Yinyanghuo, Zhimu, Danshen, Buguzhi, Xuduan, and Dihuang, respectively.

Building the compound-target network

A compound-target interaction network was constructed to illustrate the relationship between the bioactive compounds in XLGB and their potential targets (Fig. 2). This network comprised 530 nodes (55 compounds and 465 compound-target interactions) and 1452 edges. Network analysis revealed that bioactive compounds interacted with multiple targets, and several compounds targeted a single molecule, highlighting the multi-target therapeutic nature of XLGB. Additionally, the biological activity of the compounds exceeded 10, suggesting that the active compounds in XLGB contribute significantly to the biological network system (Table 2). Among these, quercetin (activity level 217) emerged as the most potent compound, followed by luteolin (level 133) and kaempferol (level 125), indicating their critical role in OA treatment through XLGB.

Identification of OA-inflammatory targets

Differential gene expression analysis of the GSE1919 database identified 1893 DEGs, with 973 upregulated and 900 downregulated genes (Fig. S1 A-B). Further, screening of the OMIM, GeneCards, and PubMed-Gene databases for “Homo sapiens” yielded 435 common targets, detailed in Table S2. Among these, 125 DEGs overlapped with inflammation-related genes, which were classified as OA-inflammatory genes.

PPI networks and hub genes

To elucidate the mechanisms via which XLGB modulates inflammation in OA, the interaction between XLGB targets and bioactive compounds was analyzed. The PPI network analysis identified 125 interaction nodes and 990 edges. By applying the degree principle, the top five ranked targets—PTGS2, IL-1β, TNF-α, IL-6, and MMP-9—were selected (Fig. 3). These hub genes were primarily involved in enzymatic processes and signaling pathways (Table 3).

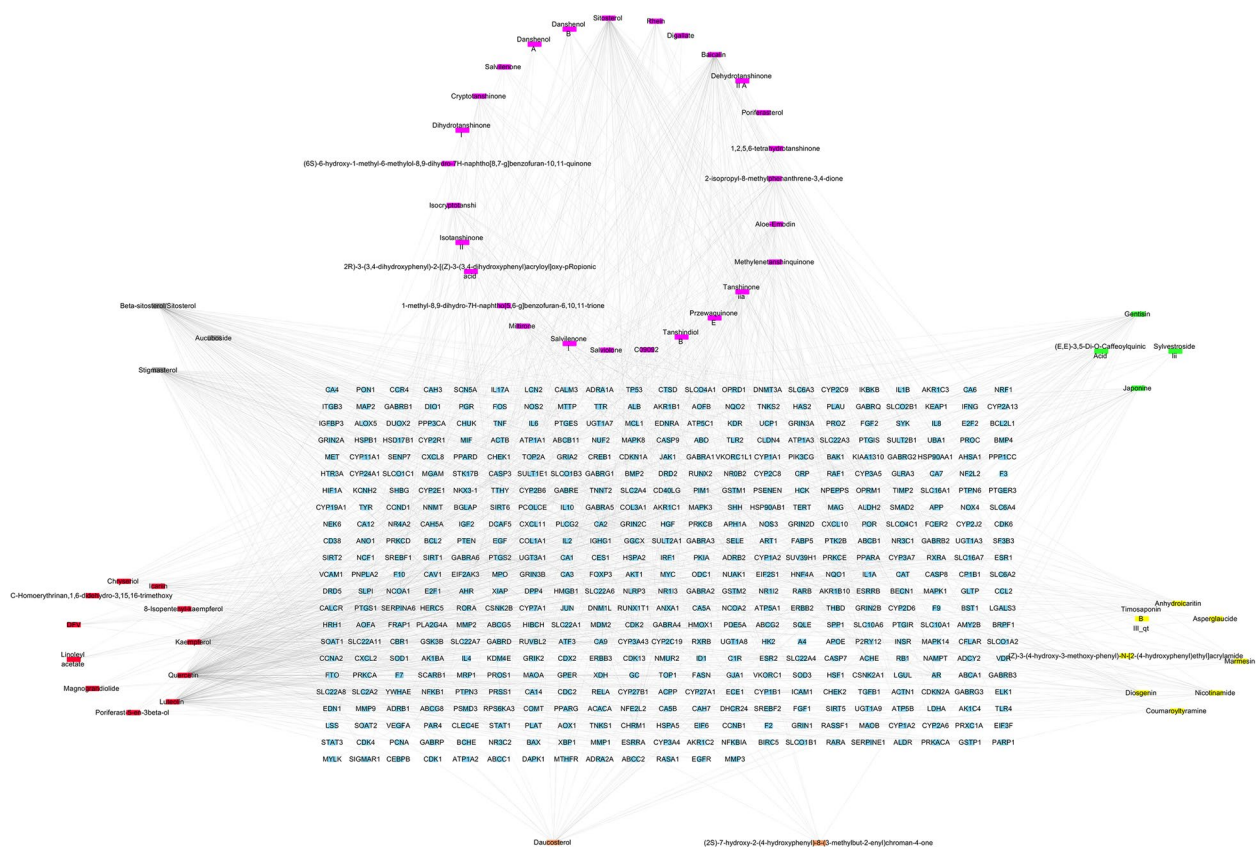


Fig. 2 Compound-target network. Blue nodes represent predicted targets; green nodes indicate Xuduan; red nodes denote Yingyanghuo; orange nodes represent Buguzhi; pink nodes depict Danshen; gray nodes represent Dihuang; yellow nodes correspond to Zhimu

Functional enrichment analysis

As depicted in Fig. 4A, the identified targets were predominantly enriched in biological processes (BP) related to biotic stimuli, oxidative stress, external stimuli, LPS, and bacterial-origin molecules. In cellular components (CC), the targets were associated with membrane rafts, membrane regions, outer membranes, mitochondrial outer membranes, transcription factor complexes, and serine/threonine protein kinases (Fig. 4B). In the molecular function (MF) category, targets were linked to cell adhesion molecule binding, cytokine interactions, nuclear hormone receptors, and phosphorylated proteins (Fig. 4C). KEGG pathway analysis revealed that DEGs were primarily enriched in the TNF signaling pathway, PI3 K-Akt signaling pathway, IL-17 signaling pathway, NF- κ B signaling pathway, chemokine signaling pathway, HIF-1 signaling pathway, Toll-like receptor signaling pathway, p53 signaling pathway, Th17 cell differentiation, and VEGF signaling pathway (Fig. 5A). These results suggest that XLGB modulates OA inflammation through multiple signaling pathways. Among these, the NF- κ B pathway plays a central role in regulating the transcription of genes involved in inflammation, immune

responses, and cell differentiation. As shown in Fig. 5B, key XLGB target proteins in the NF- κ B pathway include IL-1 β , TNF- α , IKK α , p65, I κ B α , and COX-2. IL-1 β , TNF- α , and COX-2 were selected as hub genes for further validation, while the expression of IKK α , p65, and I κ B α was assessed by immunofluorescence to elucidate XLGB's immune-regulatory effects.

Molecular docking and dynamics simulation

Molecular docking analysis revealed that all bioactive compounds in XLGB bound to key targets—IL-6, PTGS2, MMP-9, TNF- α , and IL-1 β —to varying extents, indicating that XLGB modulates OA inflammation through regulation of these targets (Fig. S2). Notably, as shown in Fig. 6A, (2R)-3-(3,4-dihydroxyphenyl)-2-[(Z)-3-(3,4-dihydroxyphenyl)acryloyl]oxy-propionic acid exhibited a strong binding affinity for PTGS2 (docking score = -9.057, binding energy = -152.75 kcal/mol) (Fig. 6A-a). Anhydroicaritin demonstrated strong binding to IL-6 (docking score = -9.176, binding energy = -26.64 kcal/mol) (Fig. 6A-b), IL-1 β (docking score = -7.64, binding energy = -102.67 kcal/mol) (Fig. 6A-c), and TNF- α (docking score = -10.007, binding energy



Gene Name	Uniprot ID	Target	Target Class	Degree
TNF- α	P01375	Tumor necrosis factor- α	Signaling	69
MMP-9	P14780	Matrix metalloprotease 9	Enzyme	59
IL-6	P05231	Interleukin-6	None	82
IL-1 β	P01584	Interleukin 1 beta	None	53
PTGS2	P35354	Prostaglandin-endoperoxide synthase 2	Enzyme	60

=−199.61 kcal/mol) (Fig. 6A-d). (2S)–7-hydroxy-2-(4-hydroxyphenyl)–8-(3-methylbut-2-enyl)chroman-4-one was found to bind to *MMP-9* (docking score = −8.454, binding energy = −81.62 kcal/mol) (Fig. 6A-e). To further validate the binding energy of these compounds with their respective targets, MD simulations were performed, and the root-mean-square deviation (RMSD), a measure of the deviation of atomic coordinates from a reference structure, was used to assess the stability of the simulation system. As shown in Fig. 6B-a, RMSD analysis of the bioactive compound-key target complexes indicated that

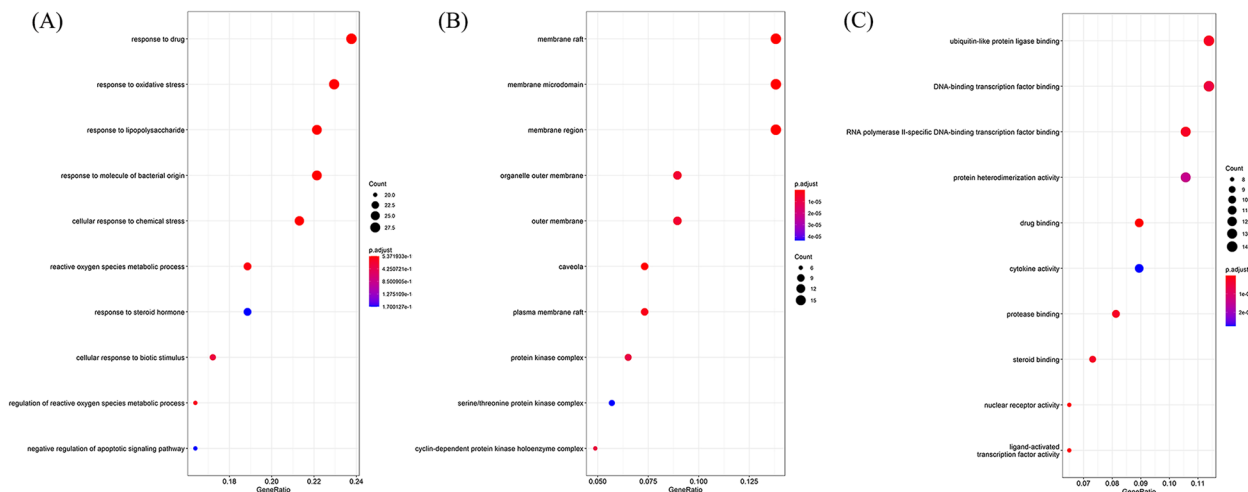


Fig. 4 GO pathway enrichment analysis. **A** Bubble chart of the top 20 biological processes (BP) associated with XLGB in OA; **B** Bubble chart of the top 20 cellular components (CC) associated with XLGB in OA; **C** Bubble chart of the top 20 molecular functions (MF) associated with XLGB in OA

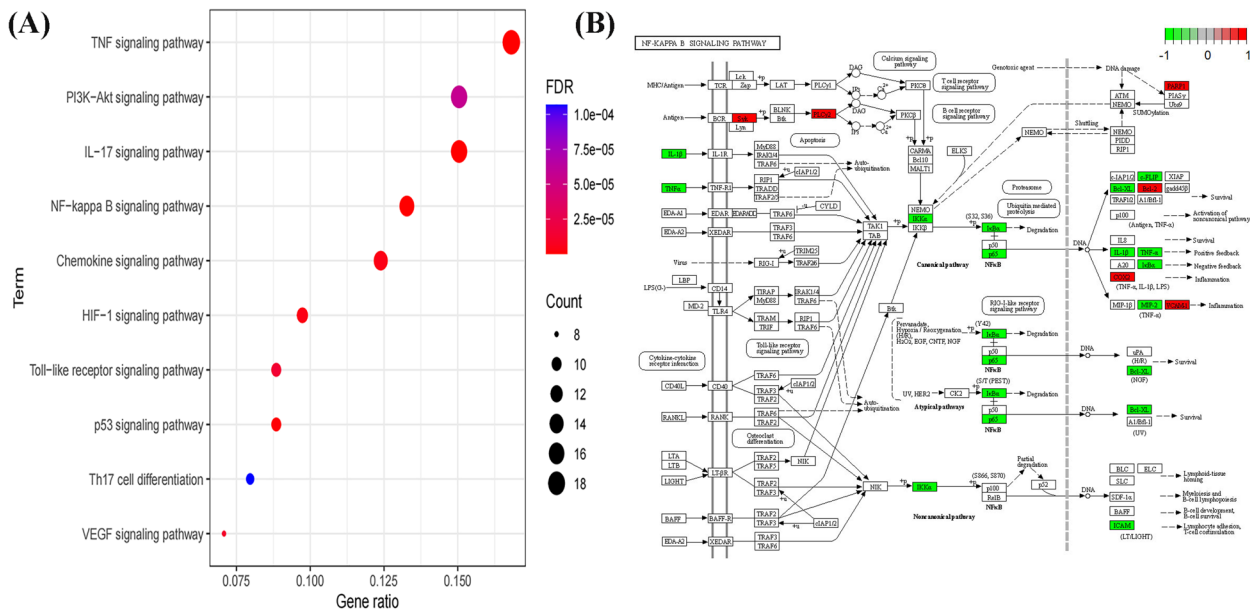


Fig. 5 KEGG pathway enrichment analysis. **A** Bubble chart of the 10 key signaling pathways related to XLGB in OA; **B** The NF-κB signaling pathway associated with XLGB treatment in OA

the protein–ligand systems reached equilibrium after 50 ns, suggesting stable binding between the bioactive compounds and their target atoms. Figure 6B-b illustrates the average number of hydrogen bonds formed between key targets and bioactive compounds: 2 for PTGS2, 5 for IL-6, 4.5 for IL-1 β , 6 for TNF- α , and 1 for MMP-9, confirming hydrogen bond interactions between proteins and ligands. Within these simulation systems, molecules with the most negative energy values (584, 913, 719, 497, 330)

played a dominant role in system stability, attributed to strong interactions such as hydrogen bonding and hydrophobic interactions. Residues A:VAL:447 (−1.70 kcal/mol), A:PHE:785 (−5.43 kcal/mol), A:ARG:596 (−2.76 kcal/mol), A:PRO:160 (−3.58 kcal/mol), and A:ILE:49 (−2.74 kcal/mol) exhibited moderately negative energy values, indicating their auxiliary role in maintaining structural integrity and potential contributions to binding (Fig. 6B-c). Collectively, these results demonstrate

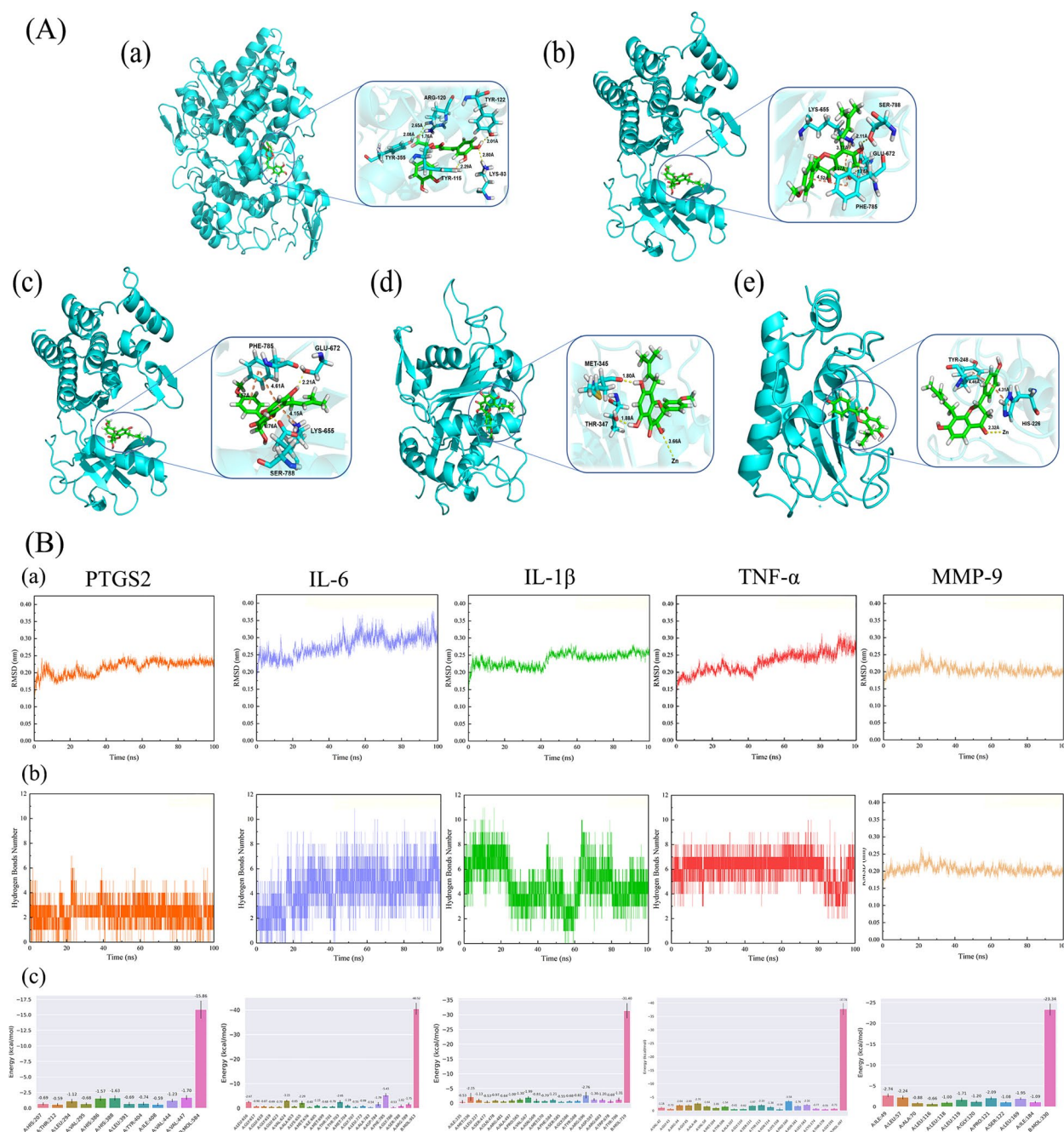


Fig. 6 Molecular docking and dynamics simulation of bioactive compound-hub target interactions. **A** Molecular docking of bioactive compounds with hub target: **(a)** (2R)-3-(3,4-dihydroxyphenyl)-2-[(Z)-3-(3,4-dihydroxyphenyl)acryloyl]oxy-propionic acid-PTGS2 (docking score = -9.057); **(b)** Anhydroicartin-IL-6 (docking score = -9.176); **(c)** Anhydroicartin-IL-1 β (docking score = -7.64); **(d)** Anhydroicartin-TNF- α (docking score = -10.007); **(e)** (2S)-7-hydroxy-2-(4-hydroxyphenyl)-8-(3-methylbut-2-enyl)chroman-4-one-MMP-9 (docking score = -8.454); **B** Molecular dynamics simulation of bioactive compound-hub target interactions: **(a)** Root-mean-square deviation (RMSD); **(b)** Intramolecular H-bond plots; **(c)** Energy contributions of residues in the molecular dynamics simulation

that the bioactive compounds in XLGB exhibit strong binding affinities with key targets (PTGS2, IL-1 β , TNF- α , IL-6, MMP-9), further validating the reliability of the predicted interactions.

Compounds present in the XLGB extract

UPLC/TOF-MS analysis was performed to identify the compounds present in XLGB extracts (Fig. 7A–B). Using retention times, primary and

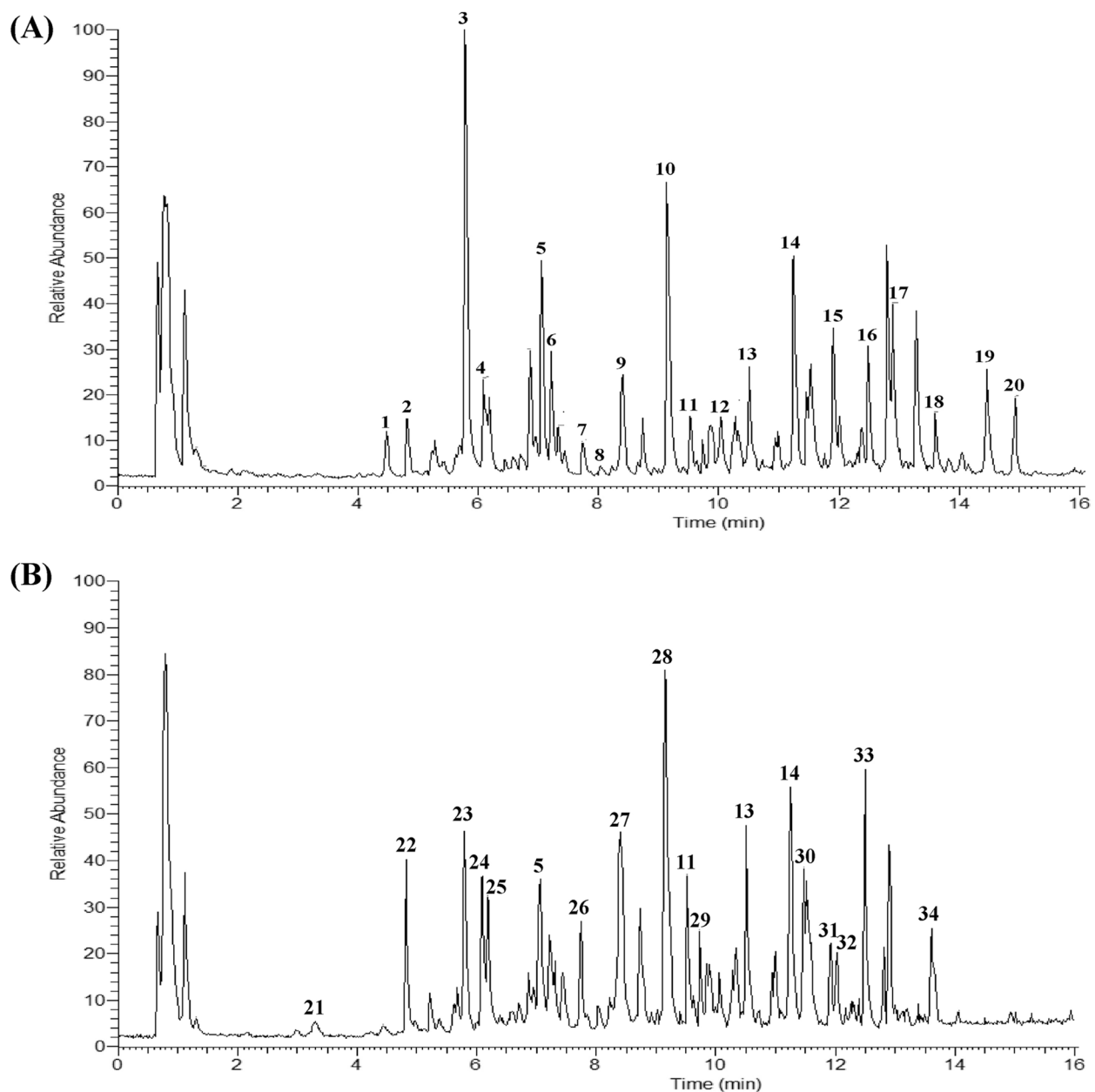


Fig. 7 UPLC/TOF-MS analysis of XLGB extract. **A** Positive mode chromatograms; **B** Negative mode chromatograms

secondary mass spectrometry data, and screening relevant literature, 34 compounds were identified, including coniferaldehyde, atenolol acid, 3-phenylpropanoic acid, 3,5-dihydroxy-2-naphthoic acid, ikarisoside C, diphyllside B, lithospermic acid, salvianolic acid, epimedin C, maslinic acid, ikarisoside B, psoralen, anhydroicaritin 3-rhamnosyl, neobavaisoflavone, flemistricin E, isobavachalcone, bavachinin, cryptotanshinone, tanshinone IIA, estra-1,3,5(10)-trien-3-ol, piscidic acid, mussaenosidic acid, sweroside,

3-acetyl-7-beta-D-glucopyranosyl-oxy coumarin, cycloolivil, epimedin A1, epimedin C, ovemotide, noranhydroicaritin-3-rhamnosyl-rhamnoside, timosaponin A-III, xanthohumol, corylin, isobavachin, and estradiol (Table 4). Many of these compounds, including neobavaisoflavone, cryptotanshinone, and tanshinone IIA, have been previously reported in *Salvia miltiorrhiza* and related medicinal herb studies [42, 43]. However, compounds such as cycloolivil and timosaponin A-III have not been widely reported in the literature, and their

Table 4 MS/MS data in (\pm) ESI modes and the identities of bioactive compounds in XLGB

NO	Ingredient	Time (min)	m/z	Mode	Formula
1	Coniferaldehyde	4.82	178.06	Positive	C ₁₀ H ₁₀ O ₃
2	Atenolol acid	4.88	267.14	Positive	C ₁₄ H ₂₁ NO ₄
3	3-Phenylpropanoic acid	5.78	150.06	Positive	C ₉ H ₁₀ O ₂
4	3,5-Dihydroxy-2-naphthoic acid	6.09	204.04	Positive	C ₁₁ H ₈ O ₄
5	Ikariside C	7.05	824.27	Positive/Negative	C ₃₈ H ₄₈ O ₂₀
6	Diphyllloside B	7.21	808.27	Positive	C ₃₈ H ₄₈ O ₁₉
7	Lithospermic acid	7.74	538.11	Positive	C ₂₇ H ₂₂ O ₁₂
8	Salvianolic acid	7.75	718.15	Positive	C ₃₆ H ₃₀ O ₁₆
9	Epimedin C	8.41	822.29	Positive	C ₃₉ H ₅₀ H ₁₉
10	Maslinic acid	9.14	472.35	Positive	C ₃₀ H ₄₈ O ₄
11	Ikariside B	9.53	662.21	Positive/Negative	C ₃₂ H ₃₈ O ₁₅
12	Psoralen	10.03	186.03	Positive	C ₁₁ H ₆ O ₃
13	Anhydrocaritin 3-rhamnosyl	10.51	660.24	Positive/Negative	C ₃₃ H ₄₀ O ₁₄
14	Neobavaisoflavone	11.25	322.11	Positive/Negative	C ₂₀ H ₁₈ O ₄
15	Flemistricin E	11.91	324.13	Positive	C ₂₀ H ₂₀ O ₄
16	Isobavachalcone	12.49	324.13	Positive	C ₂₀ H ₂₀ O ₄
17	Bavachinin	12.80	338.15	Positive	C ₂₁ H ₂₂ O ₄
18	Cryptotanshinone	13.29	296.14	Positive	C ₁₉ H ₂₀ O ₃
19	Tanshinone IIA	14.46	296.12	Positive	C ₁₉ H ₁₈ O ₃
20	Estra-1,3,5(10)-trien-3-ol	14.93	256.18	Positive	C ₁₈ H ₂₄ O
21	Piscidic acid	3.31	256.06	Negative	C ₁₁ H ₁₂ O ₇
22	Mussaenosidic acid	4.82	376.14	Negative	C ₁₆ H ₂₄ O ₁₀
23	Sweroside	5.80	358.13	Negative	C ₁₆ H ₂₂ O ₉
24	3-acetyl-7-beta-D-glucopyranosyloxycoumarin	6.10	366.10	Negative	C ₁₇ H ₁₈ O ₉
25	Cycloolivil	6.13	376.15	Negative	C ₂₀ H ₁₈ O ₉
26	Epimedin A1	7.85	838.29	Negative	C ₃₉ H ₄₈ O ₂₀
27	Epimedin C	8.40	822.29	Negative	C ₃₉ H ₅₀ O ₁₉
28	Overmotide	9.15	973.51	Negative	C ₄₆ H ₇₁ N ₉ O ₁₄
29	Noranhydrocaritin 3-rhamnosyl-rhamnoside	9.73	646.23	Negative	C ₃₂ H ₃₈ O ₁₄
30	Timosaponin A-III	11.59	740.43	Negative	C ₃₉ H ₆₄ O ₁₃
31	Xanthohumol	11.89	354.15	Negative	C ₂₁ H ₂₂ O ₅
32	Corylin	11.91	320.10	Negative	C ₂₀ H ₁₆ O ₄
33	Isobavachin	12.49	324.14	Negative	C ₂₀ H ₂₀ O ₄
34	Estradiol	13.65	272.18	Negative	C ₁₈ H ₂₄ O ₂

presence in XLGB suggests that they may contribute to its pharmacological properties. Further studies are required to fully elucidate their potential roles and confirm their significance in the therapeutic effects of XLGB.

Effect of XLGB extracts on cell viability and NO production

To determine the optimal concentration of XLGB extract, RAW264.7 cells were treated with various concentrations (20, 10, 5, 2.5 $\mu\text{g/mL}$) of the extract for 24 h, and cell viability was assessed using the CellTiter-LumiTM Kit. No significant differences were observed between the DEX group and XLGB-treated groups across all concentrations ($p > 0.05$), indicating the absence of cytotoxicity,

even at the highest dose of 20 $\mu\text{g/mL}$. In contrast, LPS treatment notably reduced cell viability, demonstrating both cytotoxic and inflammatory effects in RAW264.7 cells ($p < 0.05$). This outcome aligns with the established pro-inflammatory role of LPS, commonly used to induce inflammation in OA cell models (Fig. 8A). Additionally, LPS stimulation resulted in a significant increase in NO production compared to the control group ($p < 0.01$), confirming successful induction of inflammation. In contrast, XLGB extract treatment significantly reduced LPS-induced NO production in a dose-dependent manner. At the highest concentration (20 $\mu\text{g/mL}$), XLGB significantly decreased NO production compared to the LPS group

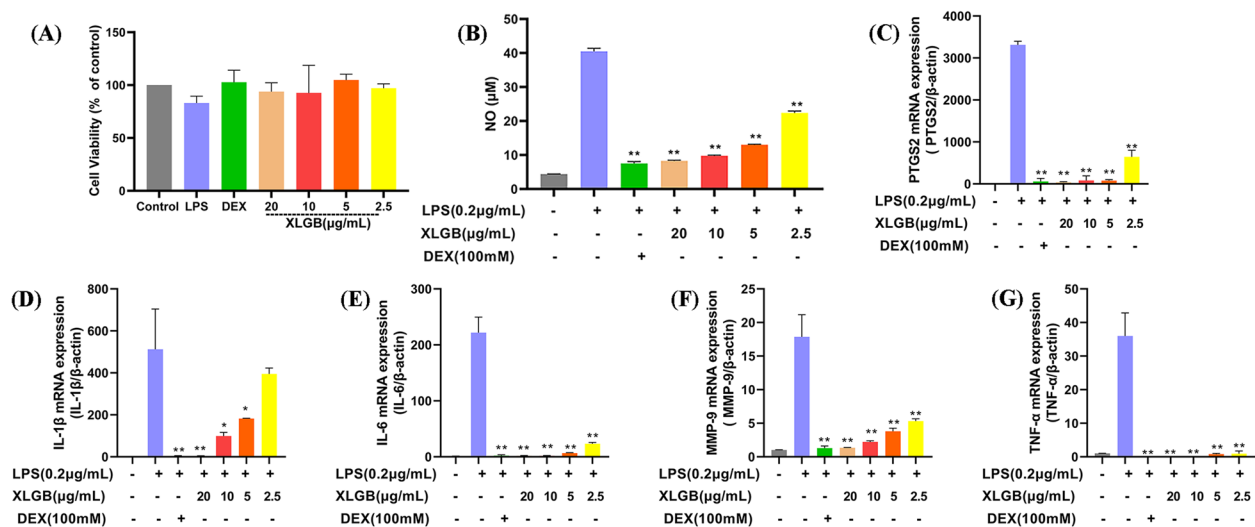


Fig. 8 Effects of XLGB extract on RAW264.7 cells. **A** Effect of XLGB extract on cell viability of RAW264.7 cells ($n = 3$); **B** Effect of XLGB extract on NO production ($n = 6$); **C** PTGS2 mRNA expression; **D** IL-1 β mRNA expression; **E** IL-6 mRNA expression; **F** MMP-9 mRNA expression; **G** TNF- α mRNA expression ($n = 3$) ($p^* < 0.05$, $**p < 0.01$)

($p < 0.01$). Similar reductions were observed at 10 $\mu\text{g/mL}$ and 5 $\mu\text{g/mL}$ ($p < 0.05$), with the lowest concentration (2.5 $\mu\text{g/mL}$) also leading to a significant decrease in NO production ($p < 0.05$), indicating XLGB's anti-inflammatory effect even at lower doses (Fig. 8B).

Effect of XLGB extract on hub genes in RAW264.7 cells

To assess the role of hub genes in the anti-inflammatory effects of XLGB, mRNA expression levels were measured in RAW264.7 cells treated with LPS. Cells were exposed to varying concentrations of XLGB extract, LPS (0.2 $\mu\text{g/mL}$), and DEX (100 mM) as a positive control. As shown in Fig. 8, LPS treatment significantly upregulated the expression of hub genes, confirming the successful induction of inflammation in RAW264.7 cells. In contrast, DEX, a known anti-inflammatory agent, effectively downregulated these genes, validating its use as a positive control. XLGB extract significantly downregulated the expression of PTGS2 (Fig. 8C), IL-1 β (Fig. 8D), IL-6 (Fig. 8E), MMP-9 (Fig. 8F), and TNF- α (Fig. 8G) in a dose-dependent manner ($*p < 0.05$, $**p < 0.01$) following LPS stimulation. At a concentration of 20 $\mu\text{g/mL}$, XLGB exhibited a significant downregulation of the hub genes, comparable to the effect of DEX. At lower concentrations (5 $\mu\text{g/mL}$ and 2.5 $\mu\text{g/mL}$), the inhibitory effects were less pronounced but still statistically significant. Notably, even at the lowest concentration (2.5 $\mu\text{g/mL}$), XLGB significantly reduced IL-1 β mRNA levels. These results indicate that while LPS upregulated hub gene expression, XLGB effectively suppressed their expression, thereby attenuating inflammation by modulating these key genes.

NF- κB nuclear translocation

Figure 9 highlights the differential expression of p65 within the NF- κB signaling pathway. To explore the mechanism through which XLGB modulates OA inflammation, the intracellular localization of p65 was examined. In untreated cells, the p65 subunit (red) was predominantly located in the cytoplasm, while in the normal group, it was found in the nucleus (blue). LPS treatment induced nuclear translocation of p65, thereby activating NF- κB transcriptional activity. This effect was counteracted by XLGB treatment (20 $\mu\text{g/mL}$), which inhibited the nuclear translocation of p65 (Fig. 9). These results suggest that the NF- κB signaling pathway regulates inflammation and tight junctions following combined LPS and XLGB treatment.

Discussion

OA is a chronic inflammatory condition characterized by progressive joint degeneration and subchondral bone remodeling. The primary goal of OA treatment is symptom management [7]. In TCM, OA is classified as a bone callus [44]. XLGB, a formulation prepared by the Miao minority group [45], is frequently prescribed for OA [46] due to its minimal side effects, diverse dosage forms, affordability, and proven efficacy. A multicenter, randomized, open-label, controlled trial demonstrated that XLGB effectively alleviates pain, improves symptoms, and enhances function in patients with OA [45]. This study aimed to elucidate the anti-inflammatory mechanism of XLGB in OA treatment by constructing an anti-inflammatory compound-OA target network,

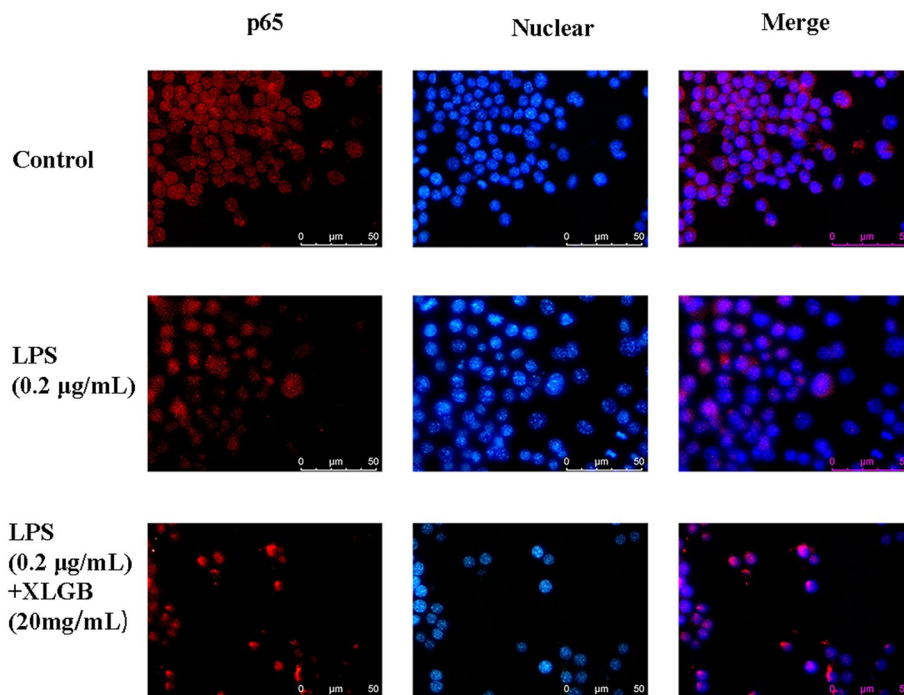


Fig. 9 Nuclear localization of the p65 subunit of NF- κ B revealed by immunofluorescence

performing functional enrichment and molecular docking analyses, and validating these findings through molecular experiments.

Fifty-five bioactive components of XLGB, including flavonoids, coumarins, saponins, alkaloids, sugars, and terpenes, met the screening criteria. The compound-target network analysis identified quercetin, luteolin, and kaempferol as key bioactive compounds with significantly higher degree values, suggesting their potential as major therapeutic targets. Quercetin, a widely recognized flavonoid, is known for its potent anti-inflammatory, antioxidant, and other beneficial properties, such as lowering blood pressure and dilating coronary arteries [47]. Research indicates that quercetin has a chondroprotective role by inhibiting the inflammatory response and apoptosis of chondrocytes, modulating synovial macrophage polarization, and fostering a pro-chondrogenic environment for chondrocytes [48]. Luteolin, a natural flavonoid found in various plants, exhibits multiple pharmacological effects, including anti-inflammatory, anti-allergy, anti-tumor, antibacterial, and antiviral activities [49]. Fei et al. [50] demonstrated that luteolin attenuates IL-1 β -induced inflammation by inhibiting the production of NO, PGE2, TNF- α , MMPs, and the phosphorylation of NF- κ B and p65. Kaempferol (OB = 41.88%, DL = 0.24, degree = 125), a bioflavonoid commonly found in fruits and vegetables, significantly inhibits IL-1 β -induced

pro-inflammatory mediators through suppression of NF- κ B signaling [51].

Analysis of the PPI network revealed 125 interaction nodes and 990 edges, highlighting the key targets associated with the anti-inflammatory effects of XLGB in OA. Topological property analysis identified five hub genes—*PTGS2*, *IL-1 β* , *TNF- α* , *IL-6*, and *MMP-9*—with the highest degree values, indicating their potential significance as anti-inflammatory targets in XLGB's treatment of OA. Inflammatory cytokines such as IL-1 β and TNF- α bind to receptors on cell membranes, increasing MMP expression, which triggers chondrocyte apoptosis and cartilage destruction [52]. IL-6, a key pro-inflammatory cytokine, plays a pivotal role in OA development and progression, explaining its elevated levels in patients with OA [53]. IL-6 also mediates the effects of IL-1 β and TNF- α , further exacerbating OA progression [54]. *PTGS2* regulates prostaglandin levels, and prostaglandin-2 increases vascular permeability, promotes inflammatory cell infiltration, and stimulates IL-6 production from chondrocytes via the NF- κ B pathway [55]. Additionally, molecular docking and dynamics simulations confirmed that core bioactive ingredients, such as anhydroicaritin, exhibited strong binding affinities with key targets, such as TNF- α and IL-6 (Fig. 6), further supporting the reliability of the predictive results.

Functional enrichment analysis indicated that all targets in the PPI network were associated with IL-17, TNF,

and NF- κ B signaling pathways. IL-17, a potent inflammatory factor, contributes to bone metabolism and disease. It modulates osteoblast differentiation and promotes bone degradation by stimulating osteoblasts and bone stromal cells [56]. Liu et al. [57] suggested that IL-17 expression correlates with the severity of KOA pain, and blocking the IL-17 signaling pathway may alleviate OA-related pain. The expression of caspase and CXCL10 was positively correlated with OA progression. Fu et al. [58] observed significantly higher caspase-3 activity in OA groups compared to sham groups. Furman et al. [59] further demonstrated that upregulation of CXCL10 plays a critical role in chronic inflammation and tissue damage following its elevation in OA cartilage. TNF, a major mediator of inflammation, downregulates inflammatory factor expression in OA synovial fibroblasts, suggesting that inhibition of the TNF signaling pathway could represent a promising strategy for OA treatment [60]. The NF- κ B pathway plays a central role in the development and persistence of OA, with previous studies indicating that NF- κ B mediates PTGS2 to regulate prostaglandin E2 (PGE2) production. Activated by pro-inflammatory cytokines like IL-1 β and TNF- α , NF- κ B forms an inflammatory feedback loop. The TNF- α /IL-1 β -NF- κ B-IL-6 axis constitutes a cascade signaling network that drives cartilage degeneration and synovial inflammation in OA [61]. Ni et al. also demonstrated that fibroblast-like synoviocytes modulate OA progression by activating the NF- κ B signaling pathway and promoting synovitis [62].

RT-PCR and immunofluorescence analyses confirmed that XLGB extract modulated the expression of predicted genes (*PTGS2*, *IL-1 β* , *TNF- α* , *IL-6*, *MMP-9*) and impacted the NF- κ B signaling pathway. LPS-induced activation of RAW264.7 macrophages, key contributors to the inflammatory response, stimulated the production of pro-inflammatory cytokines, including IL-6 and TNF- α . LPS is widely used to model inflammation-related diseases and to induce inflammatory conditions in cells. RAW264.7 macrophages play a central role in the inflammatory development of OA. LPS treatment elevated the expression of the identified hub genes (*PTGS2*, *IL-1 β* , *TNF- α* , *IL-6*, *MMP-9*), while XLGB treatment reduced their expression, demonstrating that XLGB antagonized the inflammatory effects in RAW264.7 cells in a dose-dependent manner. Wu et al. reported that Xianlinggubao, a traditional remedy for OA, exerts its effects by inhibiting chondrocyte apoptosis and inflammatory responses through the JNK and PI3 K/AKT/NF- κ B signaling pathways [63]. In contrast, this study combines bioinformatics analyses with experimental validation, revealing that XLGB reduces OA-related inflammation and suppresses the NF- κ B pathway, corroborating previous findings from a different perspective. Our study

provides significant insights supporting the clinical application of XLGB in OA treatment.

This study has several limitations. Regarding research design and methodology, the reliance on existing databases (e.g., TCMSP, ETCM) for screening active ingredients and targets may lead to the exclusion of certain XLGB constituents and novel inflammatory targets. Future research will incorporate high-resolution mass spectrometry and metabolomics to more comprehensively identify chemical entities in XLGB. While the RAW264.7 macrophage cell line served as a useful model for validating inflammatory targets, it does not fully replicate the intricate interactions present in the OA joint microenvironment. Therefore, future studies will utilize primary synovial fibroblasts derived from patients with OA or 3D organoid models to improve experimental fidelity. Additionally, the current findings, primarily based on in vitro experiments, lack in vivo validation. To address this gap, OA animal models (e.g., collagenase-induced or surgical models) will be employed in combination with micro-CT and histopathological analysis to assess XLGB's effects on cartilage degradation and bone remodeling. From a translational medicine perspective, XLGB—a multi-component traditional Chinese medicine—interacts through a complex network of constituents influencing its efficacy. Component deletion experiments or orthogonal design studies will be necessary to isolate and identify key active ingredients. Furthermore, existing clinical data do not fully account for differential efficacy across OA subtypes, highlighting the need for multi-center, stratified clinical studies.

Future research will focus on three key areas. 1. Animal Model Validation: Collagenase-induced (MIA-OA) or surgically induced (e.g., DMM) mouse OA models will be used to assess XLGB's in vivo effects on cartilage degradation, synovial inflammation, and bone remodeling. Micro-CT, histopathology (hematoxylin–eosin/Safranin O staining), and biomechanical analyses will provide quantitative assessments of joint structure and function. Gene knockout models (e.g., NF- κ B p65 conditional knockout mice) and fluorescent reporter systems will be employed to explore the regulation of signaling pathways. 2. Clinical Translation: Multi-center, randomized, double-blind, placebo-controlled RCTs (following CONSORT guidelines) will involve patients with knee/hand OA to evaluate the long-term effects on pain (VAS), function (WASOC), and inflammation (hs-CRP, IL-6). Proteomic and metabolomic profiling of biosamples (serum, synovial fluid) will identify biomarkers responsive to treatment, enabling precision stratification. 3. Mechanism & Technology: Single-cell transcriptomic sequencing (scRNA-seq) will be utilized to uncover XLGB's regulatory networks in OA joint cell

subpopulations (macrophages, synovial fibroblasts, chondrocytes), revealing immunometabolic reprogramming. Nanodelivery systems (e.g., liposomal/exosomal carriers) will enhance the bioavailability of active ingredients in joints while minimizing systemic exposure. Collectively, these strategies will deepen mechanistic understanding and enhance the translational potential of XLGB in OA treatment.

Conclusions

This study, by integrating network pharmacology with experimental validation, comprehensively elucidated how XLGB suppresses OA inflammation through the synergistic modulation of PTGS2, IL-1 β , TNF- α , IL-6, MMP-9, and the NF- κ B pathway. This provides a theoretical foundation for the multi-component, multi-target synergistic effects of TCM compounds, paving the way for developing low-side-effect treatment strategies for OA. Future research will focus on three primary objectives: first, evaluating XLGB's in vivo efficacy in OA using animal models; second, exploring XLGB's impact on immune cell subsets within the joint microenvironment using single-cell sequencing technology; and third, conducting multi-center clinical trials to assess XLGB's long-term safety and patient-stratified efficacy. These forthcoming studies will build upon the findings of the current research while providing clear guidance for future investigations.

Abbreviations

ADME	Adsorption, distribution, metabolism, and excretion
AR	Androgen receptor
BP	Biological processes
CC	Cellular components
CM	Chinese Medicine
DEGs	Differentially expressed genes
DL	Drug-likeness
DMM	Dorsal Medical Meniscectomy
EGF	Epidermal growth factor
EGFR	Epidermal growth factor receptor
ETCM	Encyclopedia of Traditional Chinese Medicine
FC	Fold change
GO	Gene Ontology
ILs	Interleukins
KEGG	Kyoto Encyclopedia of Genes and Genomes
MIA-OA	Monosodium Iodoacetate-induced OA
MD	Molecular dynamics
Micro-CT	Micro-Computed Tomography
OA	Osteoarthritis
OB	Oral bioavailability
PGE2	Prostaglandin E2
PPI	Protein-protein interaction
RA	Rheumatoid arthritis
RCT	Randomized Controlled Trial
RMSD	Root-mean-square deviation
scRNA-seq	Single-cell RNA sequencing
SEA	Similarity ensemble approach database
TCM	Traditional Chinese medicine
TCMSP	Traditional Chinese Medicine Systems Pharmacology Database and Analysis Platform
VAS	Visual Analogue scale

Supplementary Information

The online version contains supplementary material available at <https://doi.org/10.1186/s12906-025-04928-5>.

Supplementary Material 1. Table S1: Predicted targets of bioactive compounds in XLGB.

Supplementary Material 2. Table S2: Differentially expressed genes (DEGs) between OA and normal samples.

Supplementary Material 3. Figure S1: Differential gene expression analysis based on the GSE1919 database. (A) Volcano plot of DEGs comparing OA and normal samples. Red and green nodes represent upregulated and downregulated genes, respectively. (B) Heatmap of DEGs comparing samples from OA and normal groups.

Supplementary Material 4. Figure S2: Heatmaps of docking scores for hub genes activated by bioactive compounds in XLGB.

Supplementary Material 5.

Acknowledgements

We would like to thank Bullet Edits Limited for the linguistic editing and proof-reading of the manuscript.

Authors' contributions

Naiqiang Zhu and Bin Chen conceived and designed the study. Jingyi Hou performed the investigation, formal analysis and writing- original draft. Yubo Li performed the methodology, software, data curation and visualization. Ning Yang performed the experimental validation. Yu Zhang and Guiyun Ma wrote and revised the manuscript and all authors commented on previous versions of the manuscript. All authors read and approved the final manuscript.

Funding

This study was supported by the Hebei Natural Science Foundation (H2022406038) and National Natural Science Foundation of China (82305055).

Data availability

All datasets presented in this study are included in the article/Supplementary Materials.

Declarations

Ethics Statement

Not applicable.

Competing interests

The authors declare no competing interests.

Author details

¹Hebei Province Key Laboratory of Study and Exploitation of Chinese Medicine, Institute of Traditional Chinese Medicine, Chengde Medical University, Chengde, Hebei, China. ²Department of Minimally Invasive Spinal Surgery, The Affiliated Hospital of Chengde Medical University, No.36 Nanyingzi Street, Chengde, Hebei 067000, China. ³Hebei Key Laboratory of Panvascular Diseases, Chengde, Hebei, China.

Received: 27 August 2023 Accepted: 19 May 2025

Published online: 27 May 2025

References

- Naselli F, Bellavia D, Costa V, De Luca A, Raimondi L, Giavaresi G, et al. Osteoarthritis in the Elderly Population: Preclinical Evidence of Nutritional Activities of Flavonoids. *Nutrients*. 2023;16:112.
- Chen W, Wang Q, Tao H, Lu L, Zhou J, Wang Q, et al. Subchondral osteoclasts and osteoarthritis: new insights and potential therapeutic avenues. *Acta Biochim Biophys Sin (Shanghai)*. 2024;56:499–512.

3. Woodell-May JE, Sommerfeld SD. Role of Inflammation and the Immune System in the Progression of Osteoarthritis. *J Orthop Res*. 2020;38:253–7.
4. Liao CR, Wang SN, Zhu SY, Wang YQ, Li ZZ, Liu ZY, et al. Advanced oxidation protein products increase TNF- α and IL-1 β expression in chondrocytes via NADPH oxidase 4 and accelerate cartilage degeneration in osteoarthritis progression. *Redox Biol*. 2020;28: 101306.
5. Zhang W, Ouyang H, Dass CR, Xu J. Current research on pharmacologic and regenerative therapies for osteoarthritis. *Bone Res*. 2016;4:15040.
6. Nelson AE. Osteoarthritis year in review 2017: clinical. *Osteoarthritis Cartilage*. 2018;26:319–25.
7. Taruc-Uy RL, Lynch SA. Diagnosis and treatment of osteoarthritis. *Prim Care*. 2013;40(821–36):vii.
8. De Bari C, Roelofs AJ. Stem cell-based therapeutic strategies for cartilage defects and osteoarthritis. *Curr Opin Pharmacol*. 2018;40:74–80.
9. Song W, Ni S, Fu Y, Wang Y. Uncovering the mechanism of Moxing Ganshi Decoction on asthma from a systematic perspective: A network pharmacology study. *Sci Rep*. 2018;8:17362.
10. Wang X, He Y, Guo B, Tsang MC, Tu F, Dai Y, et al. In vivo screening for anti-osteoporotic fraction from extract of herbal formula Xianlinggubao in ovariectomized mice. *PLoS ONE*. 2015;10: e0118184.
11. Berger SI, Iyengar R. Network analyses in systems pharmacology. *Bioinformatics*. 2009;25:2466–72.
12. Ru J, Li P, Wang J, Zhou W, Li B, Huang C, et al. TCMSP: a database of systems pharmacology for drug discovery from herbal medicines. *J Cheminform*. 2014;6:13.
13. Xu HY, Zhang YQ, Liu ZM, Chen T, Lv CY, Tang SH, et al. ETCM: an encyclopaedia of traditional Chinese medicine. *Nucleic Acids Res*. 2019;47:D976–82.
14. Wu Y, Zhang F, Yang K, Fang S, Bu D, Li H, et al. SymMap: an integrative database of traditional Chinese medicine enhanced by symptom mapping. *Nucleic Acids Res*. 2019;47:D1110–7.
15. Bocci G, Carosati E, Vayer P, Arrault A, Lozano S, Cruciani G. ADME-Space: a new tool for medicinal chemists to explore ADME properties. *Sci Rep*. 2017;7:6359.
16. Jahid MJ, Ruan J. An Ensemble Approach for Drug Side Effect Prediction. *Proceedings (IEEE Int Conf Bioinformatics Biomed)*. 2013:440–5. <https://ieeexplore.ieee.org/document/6732532>.
17. Davies M, Nowotka M, Papadatos G, Dedman N, Gaulton A, Atkinson F, et al. ChEMBL web services: streamlining access to drug discovery data and utilities. *Nucleic Acids Res*. 2015;43:W612–20.
18. UniProt Consortium T. UniProt: the universal protein knowledgebase. *Nucleic Acids Res*. 2018;46:2699.
19. Ungethüm U, Haeupl T, Witt H, Koczan D, Krenn V, Huber H, et al. Molecular signatures and new candidates to target the pathogenesis of rheumatoid arthritis. *Physiol Genomics*. 2010;42A:267–82.
20. Law CW, Alhamdoosh M, Su S, Dong X, Tian L, Smyth GK, et al. RNA-seq analysis is easy as 1–2–3 with limma, Glimma and edgeR. *F1000Res*. 2016;17:5.
21. Pathan M, Keerthikumar S, Ang C-S, Gangoda L, Quek CYJ, Williamson NA, et al. FunRich: An open access standalone functional enrichment and interaction network analysis tool. *Proteomics*. 2015;15:2597–601.
22. Munir N, Cheng C, Xia C, Xu X, Nawaz MA, Iftikhar J, et al. RNA-Seq analysis reveals an essential role of tyrosine metabolism pathway in response to root-rot infection in *Gerbera hybrida*. *PLoS ONE*. 2019;14: e0223519.
23. Pinero J, Queralt-Rosinach N, Bravo A, Deu-Pons J, Bauer-Mehren A, Baron M, et al. DisGeNET: a discovery platform for the dynamical exploration of human diseases and their genes. *Database (Oxford)*. 2015;2015:bav028.
24. Yu G, Wang LG, Han Y, He QY. clusterProfiler: an R package for comparing biological themes among gene clusters. *OMICS*. 2012;16:284–7.
25. Zhu N, Hou J. Exploring the mechanism of action Xianlinggubao Prescription in the treatment of osteoporosis by network pharmacology. *Comput Biol Chem*. 2020;85: 107240.
26. Neese F. The ORCA program system. *WIREs Computational Molecular Science*. 2012;2:73–8.
27. Becke AD. Density-functional thermochemistry. III. The role of exact exchange. *J Chemical Physics*. 1993;98:5648–52.
28. Lee C, Yang W, Parr RG. Development of the Colle-Salvetti correlation-energy formula into a functional of the electron density. *Phys Rev B Condens Matter*. 1988;37:785–9.
29. Weigend F, Ahlrichs R. Balanced basis sets of split valence, triple zeta valence and quadruple zeta valence quality for H to Rn: Design and assessment of accuracy. *Phys Chem Chem Phys*. 2005;7:3297–305.
30. Lu T, Chen F. Multiwfn: a multifunctional wavefunction analyzer. *J Comput Chem*. 2012;33:580–92.
31. Wang J, Wolf RM, Caldwell JW, Kollman PA, Case DA. Development and testing of a general amber force field. *J Comput Chem*. 2004;25:1157–74.
32. Van Der Spoel D, Lindahl E, Hess B, Groenhof G, Mark AE, Berendsen HJC. GROMACS: fast, flexible, and free. *J Comput Chem*. 2005;26:1701–18.
33. Maier JA, Martinez C, Kasavajhala K, Wickstrom L, Hauser KE, Simmerling C. ff14SB: Improving the Accuracy of Protein Side Chain and Backbone Parameters from ff99SB. *J Chem Theory Comput*. 2015;11:3696–713.
34. Srivastava DK, Navratna V, Tosh DK, Chinn A, Sk MF, Tajkhorshid E, et al. Structure of the human dopamine transporter and mechanisms of inhibition. *Nature*. 2024;632:672–7.
35. Zheng XL, Jiang S, Ren YY, Wang SX, Xie Y, Le T, et al. High-efficient selection of aptamers by magnetic cross-linking precipitation and development of aptasensor for 1-aminohydantoin detection. *Lwt-Food Science and Technology*. 2024;199:116128–116128.
36. Holm JE, Botha EC. Leap-frog is a robust algorithm for training neural networks. *Network*. 1999;10:1–13.
37. Bussi G, Donadio D, Parrinello M. Canonical sampling through velocity rescaling. *J Chem Phys*. 2007;126: 014101.
38. Bernetti M, Bussi G. Pressure control using stochastic cell rescaling. *J Chem Phys*. 2020;153: 114107.
39. Darden T, York D, Pedersen L. Particle mesh Ewald: An $N \cdot \log(N)$ method for Ewald sums in large systems. *J Chem Phys*. 1993;98:10089–92.
40. Valdés-Tresanco MS, Valdés-Tresanco ME, Valiente PA, Moreno E. gmx_MMPBSA: A New Tool to Perform End-State Free Energy Calculations with GROMACS. *J Chem Theory Comput*. 2021;17:6281–91.
41. Hou J, Gu Y, Zhao S, Huo M, Wang S, Zhang Y, et al. Anti-Inflammatory Effects of Aurantio-Obtusin from Seed of *Cassia obtusifolia* L. through Modulation of the NF- κ B Pathway. *Molecules*. 2018;23.
42. He L, Xu C, Wang Z, Duan S, Xu J, Li C, et al. Identification of naturally occurring inhibitors in Xian-Ling-Gu-Bao capsule against the glucuronidation of estrogens. *Front Pharmacol*. 2022;13.
43. Tian S, Liu T, Jiang J, Zhao X, Fan Y, Zhang W, et al. Salvia miltiorrhiza ameliorates endometritis in dairy cows by relieving inflammation, energy deficiency and blood stasis. *Front Pharmacol*. 2024;15:1349139.
44. Xu BP, Yao M, Tian ZR, Zhou LY, Yang L, Li ZJ, et al. Study on efficacy and safety of Tong-luo Qu-tong plaster treatment for knee osteoarthritis: study protocol for a randomized, double-blind, parallel positive controlled, multi-center clinical trial. *Trials*. 2019;20:377.
45. Wang F, Shi L, Zhang Y, Wang K, Pei F, Zhu H, et al. A Traditional Herbal Formula Xianlinggubao for Pain Control and Function Improvement in Patients with Knee and Hand Osteoarthritis: A Multicenter, Randomized, Open-Label, Controlled Trial. *Evid Based Complement Alternat Med*. 2018;2018:1827528.
46. Chen W, Du S, Wu Q, Wu H, Chen X [Comparative study on dissolution of Xianlinggubao capsules prepared by different processes]. *Zhongguo Zhong Yao Za Zhi*. 2010;35:1541–6.
47. Marunaka Y, Marunaka R, Sun H, Yamamoto T, Kanamura N, Inui T, et al. Actions of Quercetin, a Polyphenol, on Blood Pressure. *Molecules*. 2017;22.
48. Hu Y, Gui Z, Zhou Y, Xia L, Lin K, Xu Y. Quercetin alleviates rat osteoarthritis by inhibiting inflammation and apoptosis of chondrocytes, modulating synovial macrophages polarization to M2 macrophages. *Free Radic Biol Med*. 2019;145:146–60.
49. Nabavi SF, Braidly N, Gortzi O, Sobarzo-Sanchez E, Daglia M, Skalicka-Wozniak K, et al. Luteolin as an anti-inflammatory and neuroprotective agent: A brief review. *Brain Res Bull*. 2015;119(Pt A):1–11.
50. Fei J, Liang B, Jiang C, Ni H, Wang L. Luteolin inhibits IL-1 β -induced inflammation in rat chondrocytes and attenuates osteoarthritis progression in a rat model. *Biomed Pharmacother*. 2019;109:1586–92.
51. Zhuang Z, Ye G, Huang B. Kaempferol Alleviates the Interleukin-1 β -Induced Inflammation in Rat Osteoarthritis Chondrocytes via Suppression of NF- κ B. *Med Sci Monit*. 2017;23:3925–31.
52. Beklen A, Ainola M, Hukkanen M, Gurgan C, Sorsa T, Kontinen YT. MMPs, IL-1, and TNF are regulated by IL-17 in periodontitis. *J Dent Res*. 2007;86:347–51.

53. Laavola M, Leppanen T, Hamalainen M, Vuolteenaho K, Moilanen T, Nieminen R, et al. IL-6 in Osteoarthritis: Effects of Pine Stilbenoids. *Molecules*. 2018;24.
54. Li L, Lan J, Ye Y, Yang B, Yang X, Cai Z. CPEB1 Expression Correlates with Severity of Posttraumatic Ankle Osteoarthritis and Aggravates Catabolic Effect of IL-1beta on Chondrocytes. *Inflammation*. 2019;42:628–36.
55. Tang SC, Liao PY, Hung SJ, Ge JS, Chen SM, Lai JC, et al. Topical application of glycolic acid suppresses the UVB induced IL-6, IL-8, MCP-1 and COX-2 inflammation by modulating NF-kappaB signaling pathway in keratinocytes and mice skin. *J Dermatol Sci*. 2017;86:238–48.
56. Chen B, Deng Y, Tan Y, Qin J, Chen LB. Association between severity of knee osteoarthritis and serum and synovial fluid interleukin 17 concentrations. *J Int Med Res*. 2014;42:138–44.
57. Liu Y, Peng H, Meng Z, Wei M. Correlation of IL-17 Level in Synovia and Severity of Knee Osteoarthritis. *Med Sci Monit*. 2015;21:1732–6.
58. Fu D, Shang X, Ni Z, Shi G. Shikonin inhibits inflammation and chondrocyte apoptosis by regulation of the PI3K/Akt signaling pathway in a rat model of osteoarthritis. *Exp Ther Med*. 2016;12:2735–40.
59. Furman BD, Kent CL, Huebner JL, Kraus VB, McNulty AL, Guilak F, et al. CXCL10 is upregulated in synovium and cartilage following articular fracture. *J Orthop Res*. 2018;36:1220–7.
60. Li H, Xie S, Qi Y, Li H, Zhang R, Lian Y. TNF-alpha increases the expression of inflammatory factors in synovial fibroblasts by inhibiting the PI3K/AKT pathway in a rat model of monosodium iodoacetate-induced osteoarthritis. *Exp Ther Med*. 2018;16:4737–44.
61. Yao Q, Wu X, Tao C, Gong W, Chen M, Qu M, et al. Osteoarthritis: pathogenic signaling pathways and therapeutic targets. *Signal Transduct Target Ther*. 2023;8:56.
62. Ni S, Miao K, Zhou X, Xu N, Li C, Zhu R, et al. The involvement of follistatin-like protein 1 in osteoarthritis by elevating NF-kappaB-mediated inflammatory cytokines and enhancing fibroblast like synoviocyte proliferation. *Arthritis Res Ther*. 2015;17:91.
63. Wu X, Sun S, Wu X, Sun Z. Multitech-Based Study on Medicinal Material Basis and Action Mechanism of Herbal Formula Xian-Ling-Gu-Bao Capsule in Treatment of Osteoarthritis. *Evid Based Complement Alternat Med*. 2022;2022:6986372.

Publisher's Note

Springer Nature remains neutral with regard to jurisdictional claims in published maps and institutional affiliations.